

From Chiral Fluctuations to the Skyrmion Lattice Phase in MnSi: A SANS and Neutron Spin Echo Study

C. Pappas,^{1,*} L.J. Bannenberg,¹ E. Lelièvre-Berna,² F. Qian,¹

C. Dewhurst,² D. Schlagel,³ T. A. Longrasso,³ and P. Falus²

¹*Delft University of Technology, Mekelweg 15, 2629 JB Delft, Netherlands*

²*Institut Laue-Langevin, 71 Avenue des Martyrs, CS 20156 Grenoble, France*

³*Ames Laboratory, Iowa State University, Ames, IA 50011, USA*

(Dated: November 15, 2021 version 3.0)

We present a comprehensive study of the magnetic field influence on the chiral fluctuations in the reference helimagnet MnSi by combining Small Angle Neutron Scattering and Neutron Spin Echo spectroscopy. Skyrmion lattice, conical phase and magnetic fluctuations appear to partly coexist in the A-phase. Additionally, we find that the Skyrmion lattice scattering extends over a much larger temperature region than assumed so far. Magnetic fields that stabilize the A-phase do not alter the chiral magnetic fluctuations above T_C while the first order phase transition crosses over to a less sharp transition for magnetic fields higher than 0.4 T.

Keywords: Critical phenomena, chiral magnetism, Small Angle Neutron Scattering, Neutron Spin Echo spectroscopy, Polarized Neutrons, Skyrmions.

In the reference chiral magnet MnSi, the competition between magnetic interactions and an external magnetic field stabilizes complex spin modulations including Skyrmion lattice (SkL) correlations. Skyrmions are topologically protected vortex-like spin textures that have been observed both in reciprocal space by small angle neutron scattering and in real space by Lorentz Transmission microscopy [1–7]. In MnSi, similar to other systems of the same family, the Skyrmion lattice phase is stabilized in the so-called A-Phase, a small pocket below T_C in the temperature-magnetic field phase diagram [3].

As a first approach, the ground state of MnSi and other B20 compounds can be understood by considering three hierarchically ordered interaction terms [8]: the strongest ferromagnetic exchange interaction aligns the spins, a weaker Dzyaloshinskii-Moriya (DM) term [9, 10] arises from the lack of inversion symmetry of the B20 lattice and twists the spins to a helix, whereas the weakest anisotropy term fixes the directions of the helices on the crystallographic lattice. Below the first order transition at $T_C \sim 29$ K, the ground state is a single domain left-handed helix with a pitch of $\ell \sim 17.5$ nm, and with the magnetic moments perpendicular to the helix propagation vector $\vec{\tau}$ that points along the $\langle 111 \rangle$ crystallographic directions [11]. In the helical phase an external magnetic field B exceeding the critical field B_{C1} overcomes the anisotropy and aligns the helices along its direction inducing the conical phase. Subsequently much higher fields are required, exceeding the upper critical field B_{C2} , to overcome the DM interactions and ferromagnetically align the spins inducing the spin-polarized state. The Skyrmion lattice phase is stabilized slightly below T_C and for intermediate magnetic fields between B_{C1} and B_{C2} .

An intriguing feature in MnSi is the intense diffuse neutron scattering that appears at zero field just above T_C and spreads homogeneously over the surface of a sphere

with radius $\tau = 2\pi/\ell$. This precursor phase bears similarities with liquid crystals for which a theory has been developed by Brazovskii [12] that has been applied to MnSi [13]. Spherical Neutron Polarimetry and Neutron Spin Echo (NSE) spectroscopy show that this scattering is due to chiral fluctuations, a particular topology which may be identified with a spin liquid Skyrmion state [14, 15].

In the following we will address the open question of the evolution of these chiral fluctuations and the precursor phase above T_C under magnetic fields high enough to stabilize the Skyrmion lattice phase and beyond. For this purpose, we combined Small Angle Neutron Scattering (SANS) and Neutron Spin Echo (NSE) spectroscopy. With SANS we measured the static structure factor $S(Q) \equiv S(Q, t = 0)$, with Q the momentum transfer, which is the spatial Fourier transform of the correlations. For fluctuating correlations decaying exponentially with distance d , typically $\sim \exp(-d/\xi)/d$ with ξ the characteristic correlation length, $S(Q)$ assumes the general Ornstein-Zernike form:

$$S(Q) = C / \left((Q - \tau)^2 + \xi^{-2} \right). \quad (1)$$

NSE spectroscopy determines directly the normalized intermediate scattering function $I(Q, t) = S(Q, t)/S(Q)$, thus the decay in time of the fluctuations. The combination of these two neutron scattering techniques thus provides a complete characterization of the magnetic correlations both in space and in time.

The measurements were performed on a almost cubic single crystal of MnSi with dimensions $\sim 5 \times 5 \times 5$ mm³. The crystal was grown from a stoichiometric melt as described in [16] and its structure was tested by X-ray diffraction. Laue patterns using highly penetrating (150–200 KeV) γ -rays revealed a mosaicity of $\sim 0.2^\circ/\text{mm}$. The crystal was aligned with the $[1\bar{1}0]$ axis vertical.

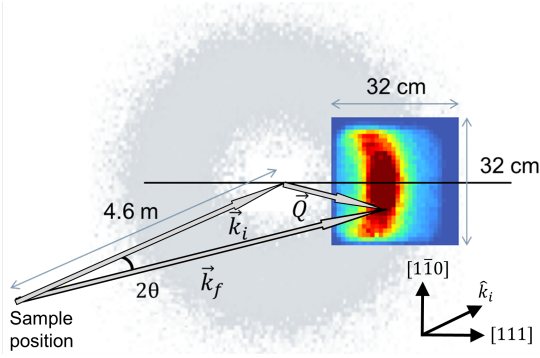


FIG. 1. Schematic drawing of the scattering geometry on IN15 with θ the scattering angle, \vec{k}_i and \vec{k}_f the incoming and scattered neutron beam wavevectors respectively and \vec{Q} the scattering vector. The 32x32 cm² detector was at 4.6 m from the sample. The magnetic field was applied either parallel or perpendicular to \vec{k}_i .

The neutron scattering experiments were performed on the instruments D33 and IN15 of the Institute Laue Langevin. On the SANS instrument D33 the neutron beam was unpolarized and incident wavelengths of $\lambda = 0.46$ nm and 0.55 nm with $\Delta\lambda/\lambda \sim 10\%$ were used. The magnetic field was applied along the wavevector of the incoming beam \vec{k}_i using an electromagnet that did not reach magnetic fields higher than 0.25 T and had a limited angular acceptance. The SANS patterns were normalized to standard monitor counts and background corrected using a measurement at 100 K.

The NSE spectrometer IN15 has a highly polarized incident neutron beam and polarization analysis capabilities but restricted angular acceptance of the 32x32 cm², with 1 cm² pixel resolution, position sensitive detector. Hence, only a fraction of the scattered beam could be recorded as illustrated by Fig. 1. The measurements were performed for $\lambda = 0.9$ and 0.8 nm, $\Delta\lambda/\lambda \sim 15\%$, using a horizontal crymagnet. The magnetic field was applied either parallel to \vec{k}_i or perpendicular to it. The NSE spectra were recorded in the ferromagnetic NSE configuration [17, 18] and were averaged over the entire detector since no significant Q -dependence was found.

We first discuss the SANS results. Fig. 2(a) depicts typical SANS patterns for $B = 0.18$ T, a field that stabilizes the Skyrmion lattice, and for $\vec{B} \parallel \vec{k}_i$, a configuration that leads to the characteristic six-fold symmetric scattering patterns [3]. The characteristic ring of diffuse scattering, similar to the one seen at zero field, is clearly present above $T_C \sim 28.8$ K. This feature broadens and decreases in intensity with increasing temperature.

Below T_C , between 28 and 28.5 K, the characteristic and intense SkL six-fold pattern appears superposed to the ring of diffuse scattering that remains clearly visible. Additional peaks which much lower intensity than the

six main peaks are also visible in the patterns. An additional measurement with an attenuated direct neutron beam revealed that the intensity of each of the Skyrmion lattice Bragg peaks at 28.25 K amounted to $\alpha = 0.4\%$ of the direct beam intensity. At the same temperature and after correction of the diffuse scattering background, the most intensive additional peaks at $Q = 0.60$ nm⁻¹ amount to $\beta = 0.6\%$ of the SkL Bragg peaks. Multiple scattering would lead to $\beta \sim 2\alpha$, which is compatible with our results. Therefore, the scattering of the 5 mm thick sample used in this experiment does not allow us to distinguish between multiple scattering and the high-order Bragg peaks previously reported by [19].

Below 28 K, the scattered intensity drops rapidly, as expected for the conical phase in which the helices are aligned by the field and hence do not fulfil the Bragg condition. However, the six-fold symmetric pattern remains visible as well as a ring of diffuse scattering. Fig. 2(b) displays the temperature dependence of the six-fold pattern *only*, i.e. after subtraction of the diffuse scattering determined next to the peaks as illustrated in Fig. S1 of the supplement. The SkL scattering is maximum in the A-phase but the intensity persists, although weak, at temperatures as low as 25 K. This is a much wider temperature range than reported so far [3] and possibly a paradigm for the extended SkL phase that has been predicted to exist also in bulk MnSi [20].

The effect of the magnetic field orientation with respect to \vec{k}_i was investigated on IN15. As shown in Fig. 3 (a) and (b), a clear difference in the scattered intensities emanates only below T_C . When the field was applied along \vec{k}_i , a configuration sensitive to helical modulations perpendicular to the field, the SkL scattering is clearly visible by the increase in intensity between 28 and 28.8 K shown by the full dots in Fig. 3 (a) and (b). On the other hand, when the field was applied perpendicular to \vec{k}_i , the Bragg condition was fulfilled by helical modulations oriented along the magnetic field revealing the scattering of the conical phase, which is seen in the strong increase of scattered intensity below T_C shown by the full squares of Fig. 3 (a) and (b). The observation of scattered intensity in the A-phase for both orientations of the magnetic field indicates the co-existence of SkL and conical correlations. A similar behavior has been observed before, most prominently over a broad temperature range, in the chiral magnet Fe_{0.7}Co_{0.3}Si [21].

Above T_C , the total scattered intensity is the same for both magnetic field orientations, which indicates that also at these high magnetic fields the diffuse scattering is homogeneously distributed over the surface of a sphere with radius τ . A radial averaging of the D33 and IN15 SANS patterns gives the scattered intensity as a function of Q , of which an example is displayed in Fig. S2(a) of the supplement. A subsequent fit with the Ornstein-Zernike relation of eq. 1 convoluted with the Gaussian instrumental resolution provides the correlation lengths displayed

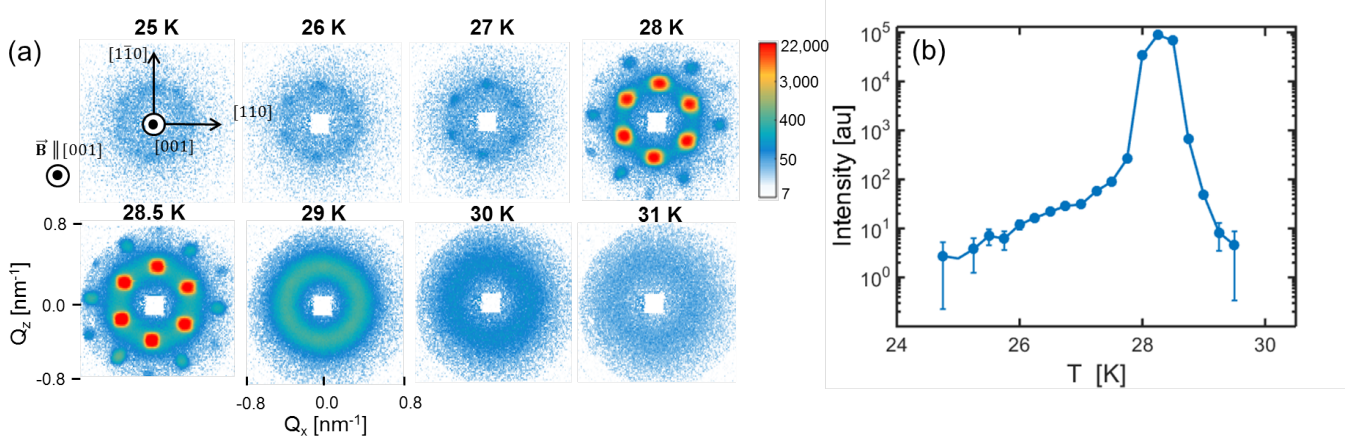


FIG. 2. (a) SANS scattering patterns obtained on D33 for a magnetic field of 0.18 T, applied along the neutron beam and perpendicular to the detector plane. (b) Scattered intensity due to the Skymion Lattice *only* as a function of temperature, i.e. after subtraction of the diffuse scattering intensity.

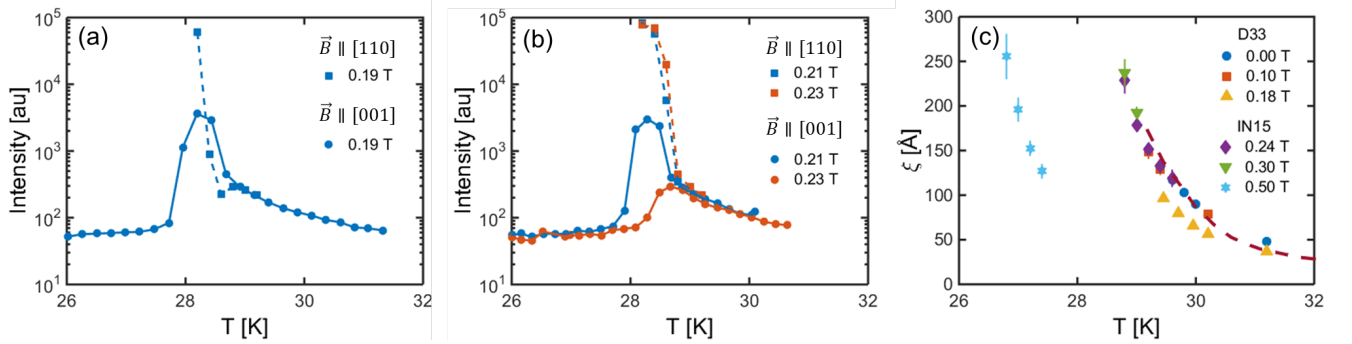


FIG. 3. Total scattered intensity as a function of temperature measured in IN15 for different orientations of the magnetic field at (a) 0.19 T and (b) 0.21 and 0.23 T. Panel (c) displays the correlation length ξ as a function of temperature above T_C for different magnetic fields. The dashed line corresponds to the Brazovskii behavior proposed by [13].

in Fig. 3(c). At zero field, these are in good agreement with values reported in the literature [13–15, 22]: ξ increases monotonously from ~ 3 nm at $T_C + 2$ K up to the approximately the pitch of the helix at T_C . This temperature dependence can be described by the analytical relation based on Brazovskii's approach provided in [13] and stays almost unchanged for all fields up to $B \sim 0.4$ T. Thus the magnetic field has a weak effect on the magnetic correlations above T_C , which is in contrast to the complex phase diagram, including the Skymion lattice phase, that it generates below T_C .

A contour plot showing the total scattered intensity as function of the temperature and magnetic field as measured on IN15 with the field *along* the incident neutron beam is given in Fig. 4. The phases that have been reported in the literature (e.g. [3, 23]) can be easily identified: at low magnetic fields the high intensity originates from the Bragg peaks of the helical phase. Magnetic fields beyond ~ 0.05 T align the helices towards their

direction and induce the conical phase, resulting in almost zero scattered intensity. The A-phase is characterized by the strong increase in intensity seen in a narrow pocket below T_C . Above T_C a similar gradual decrease of the intensity with increasing temperature is seen for all fields up to $B \sim 0.3$ T. For higher fields, this intensity decreases gradually and weakens considerably above ~ 0.4 T.

We now switch to the NSE results, which were measured at twelve magnetic fields ($0.12 \leq B \leq 0.5$) applied perpendicular to \vec{k}_i . This configuration was chosen as it is the only one that does not depolarize the scattered neutron beam in the presence of chiral correlations [24, 25]. Indeed, in the configuration $B \parallel \vec{k}_i$ the scattered beam was completely depolarized up to the highest magnetic fields applied, which indicates that the probed correlations remain completely chiral reflecting the same topology as at zero field [14, 15].

Fig. 5(a) and (b) display NSE spectra for $B = 0.24$ T

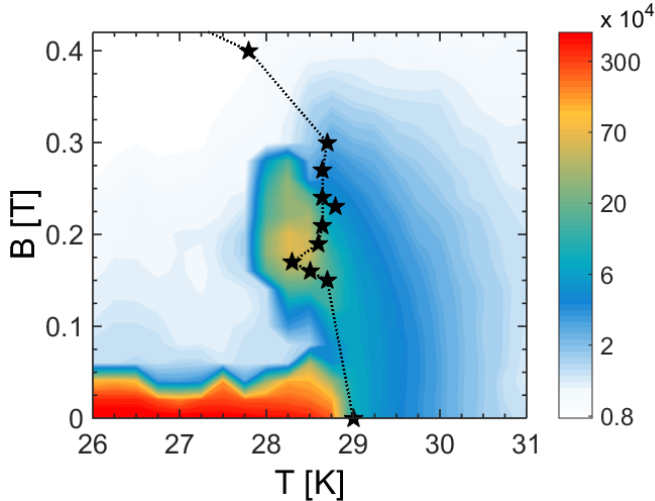


FIG. 4. Contour plot of the total scattered intensity in the configuration where $\vec{B} \parallel \vec{k}_i$ as measured on IN15 with an incident wavelength of $\lambda = 0.8$ nm. The stars indicate the highest temperatures for which the NSE spectra are 100% elastic. The evolution of the scattered intensity as a function of temperature for all magnetic fields is displayed in Fig. S3 of the supplementary information.

and $B = 0.5$ T respectively. The intermediate scattering function decays exponentially with a characteristic relaxation time t_0 to an elastic fraction a that originates from the elastic contribution of the emerging Bragg peak:

$$I(Q, t) = (1 - a) \exp(-t/t_0) + a. \quad (2)$$

For all magnetic fields up to 0.4 T, a evolves from $\sim 30\%$ to 100% within 0.2 K following the fast increase of the Bragg peak intensity with decreasing temperature displayed in Fig. 3, and which is quantitatively similar to the zero field behavior [14, 15]. A qualitative change sets-in at 0.4 T and at 0.5 T where the elastic fraction increases much slower from $\sim 30\%$ to 100% within about 0.8 K.

A similar picture is found for the relaxation times, of which a selection is depicted in Fig. 5(c). For magnetic fields lower than 0.4 T, t_0 increases from ~ 0.4 ns at $T_C + 1.5$ K to ~ 1 ns close to T_C , which is very similar to the behavior observed at zero field [14, 15]. For $B = 0.5$ T, however, a different temperature dependence is observed, where t_0 is as low as 0.1 ns at 27.4 K a temperature, where the elastic fraction is already $\sim 20\%$. In addition t_0 depends much stronger on the temperature than at the lower fields as it changes from ~ 0.1 ns to ~ 1.2 ns within 0.8 K.

The NSE results complement the contour plot of Fig. 4, where the stars indicate the highest temperatures for which the NSE spectra are 100% elastic. The points shift slightly inwards in the region of the A-phase ($0.15 \text{ T} \leq B \leq 0.24 \text{ T}$), where the strong Skyrmion lattice scat-

tering has been observed. This implies that the A-phase also coexists with magnetic fluctuations and provides an additional hint for the non-homogenous character of this phase, a feature that has been overlooked so far.

For $B \lesssim 0.4$ T the transition from the (low temperature) ordered phase to the (high temperature) chiral fluctuating phase is the same as at zero field: sharp changes occur within a very narrow temperature region of ~ 0.2 K in line with a first order phase transition. On the other hand the transition becomes less sharp and stretches over a wide temperature range for $B \gtrsim 0.4$ T, where the phase boundary is between the (low temperature) conical phase and the (high temperature) field polarized state [23]. A similar change of behavior has been reported by specific heat [23] and magnetic susceptibility [26] and has been attributed to the existence of a tricritical point where the order of the transition changes from first to second. At such a tricritical point one would expect both coefficients of the Landau free-energy functional ($F = aM^2 + bM^4 + \dots$), a and b , to become zero simultaneously. This would lead to a flat energy minimum and would possibly boost and soften the magnetic fluctuations [27], a feature that is not confirmed by our NSE spectra that probe selectively the helical correlations at $Q = \tau$. Our observations rather support a smooth cross-over from a sharp first order phase transition for $B \lesssim 0.4$ T to a gradual one for $B \gtrsim 0.4$ T.

In the absence of a tricritical point, demagnetization effects may be at the origin of the observed smooth cross-over, as they lead to non-homogeneous internal magnetic fields when the sample shape is not an ideal ellipsoid. We note that all single MnSi single crystals investigated so far are not ideal ellipsoids and that the change of behavior coincides with the change of slope of the transition line in the $B - T$ phase diagram. Below 0.4 T, this line is almost vertical and a distribution of internal magnetic fields due to the demagnetizing field should not affect the critical behavior. On the other hand for $B \gtrsim 0.4$ T a slope sets-in, in which case a distribution of internal magnetic fields smears the critical behavior inversely proportionally to the absolute value of the slope, in agreement with our observations. This could also explain the specific heat results [23] as well as the sample shape dependence of the magnetic phase diagram observed by dc magnetization and ac susceptibility measurements [28]. Only experiments on ideal ellipsoid shaped samples could therefore set the debate on the phase diagram of MnSi and the possible existence of a tricritical point.

In addition, our results show that chiral fluctuations above T_C persist up to at least 0.5 T and that the precursor phase is less affected by the magnetic field than the low temperature ordered (helical, conical or A-) phases. Furthermore, we find that the Skyrmion lattice scattering extends over a much higher temperature region than assumed so far and that in the A-phase it coexists with the conical phase and magnetic fluctuations. Thus mul-

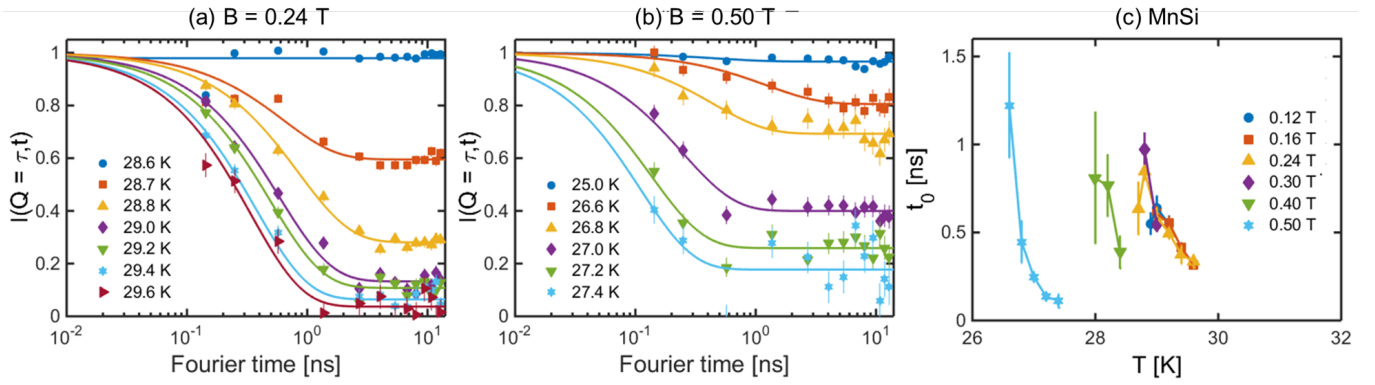


FIG. 5. Neutron Spin Echo spectroscopy results. Panel (a) and (b) show the intermediate scattering function $I(Q, t)$ measured at (a) 0.24 T and (b) 0.5 T. Panel (c) shows the deduced relaxation times t_0 as a function of temperature for the magnetic fields indicated.

multiple phases may co-exist simultaneously, metastable or in thermodynamic equilibrium with each other, even in the archetype chiral magnet MnSi.

The authors thank P. Courtois for testing the MnSi single crystal with γ -ray Laue diffraction and Bob Cubitt for his input on the SkL Bragg peak intensity analysis. They also acknowledge fruitful discussions with M. Mostovoy, G.R. Blake and T. Palstra. LB acknowledges financial support by NWO Groot project LARMOR 721.012.102 and FQ from the China Scholarship Council. DL and TL acknowledge the support of the the US Department of Energy (DOE), Office of Science, Basic Energy Sciences, Materials Science and Engineering Division under Contract No. DE-AC02-07CH11358.

* c.pappas@tudelft.nl

- [1] A. Bogdanov and D. Yablonskii, *Zh. Eksp. Teor. Fiz* **95**, 182 (1989).
- [2] U. K. Röbler, A. N. Bogdanov, and C. Pfleiderer, *Nature* **442**, 797 (2006).
- [3] S. Mühlbauer, B. Binz, F. Jonietz, *et al.*, *Science* **323**, 915 (2009).
- [4] W. Münzer, A. Neubauer, T. Adams, *et al.*, *Phys. Rev. B* **81**, 041203 (2010).
- [5] X. Yu, Y. Onose, N. Kanazawa, J. Park, *et al.*, *Nature* **465**, 901 (2010).
- [6] X. Z. Yu, N. Kanazawa, Y. Onose, K. Kimoto, W. Z. Zhang, S. Ishiwata, Y. Matsui, and Y. Tokura, *Nature Materials* **10**, 106 (2010).
- [7] N. Nagaosa and Y. Tokura, *Nature Nanotechnology* **8**, 899 (2013).
- [8] P. Bak and M. H. Jensen, *J. Phys. C* **13**, L881 (1980).
- [9] I. E. Dzyaloshinski, *J. Phys. Chem. Solids* **4**, 241 (1958).
- [10] T. Moriya, *Phys. Rev* **120**, 91 (1960).
- [11] G. Shirane *et al.*, *Phys. Rev. B* **28**, 6251 (1983).
- [12] S. A. Brazovskii, *Soviet Physics JETP* **41**, 85 (1975).
- [13] M. Janoschek, M. Garst, *et al.*, *Phys. Rev. B* **87**, 05 (2013).
- [14] C. Pappas, E. Lelièvre-Berna, P. Falus, *et al.*, *Phys. Rev. Lett.* **102**, 197202 (2009).
- [15] C. Pappas, E. Lelièvre-Berna, P. Bentley, P. Falus, P. Fouquet, and B. Farago, *Phys. Rev. B* **83**, 224405 (2011).
- [16] S. M. Stishov, A. E. Petrova, S. Khasanov, *et al.*, *Phys. Rev. B* **76**, 052405 (2007).
- [17] B. Farago and F. Mezei, *Physica B+ C* **136**, 100 (1986).
- [18] C. Pappas, E. Lelièvre-Berna, P. Bentley, *et al.*, *Nuclear Instruments and Methods in Physics Research Section A* **592**, 420 (2008).
- [19] T. Adams, S. Mühlbauer, C. Pfleiderer, *et al.*, *Phys. Rev. Lett.* **107**, 217206 (2011).
- [20] M. Wilson, A. Butenko, A. Bogdanov, and T. Monchisky, *Phys. Rev. B* **89**, 094411 (2014).
- [21] L. Bannenberg, K. Kakurai, F. Qian, and others., submitted to *Phys. Rev. B* (2016).
- [22] S. V. Maleyev, *Phys. Rev. B* **73**, 174402 (2006).
- [23] A. Bauer, M. Garst, and C. Pfleiderer, *Phys. Rev. Lett.* **110**, 177207 (2013).
- [24] M. Blume, *Phys. Rev.* **130**, 1670 (1963).
- [25] S.V. Maleyev, V. G. Baryakhtar, and R. A. Suris, *Sov. Phys. Solid State* **4**, 2533 (1963).
- [26] L. Zhang, D. Menzel, C. Jin, *et al.*, *Phys. Rev. B* **91**, 024403 (2015).
- [27] M. Mostovoy, Private Communication (2016).
- [28] A. Bauer and C. Pfleiderer, *Phys. Rev. B* **85**, 214418 (2012).

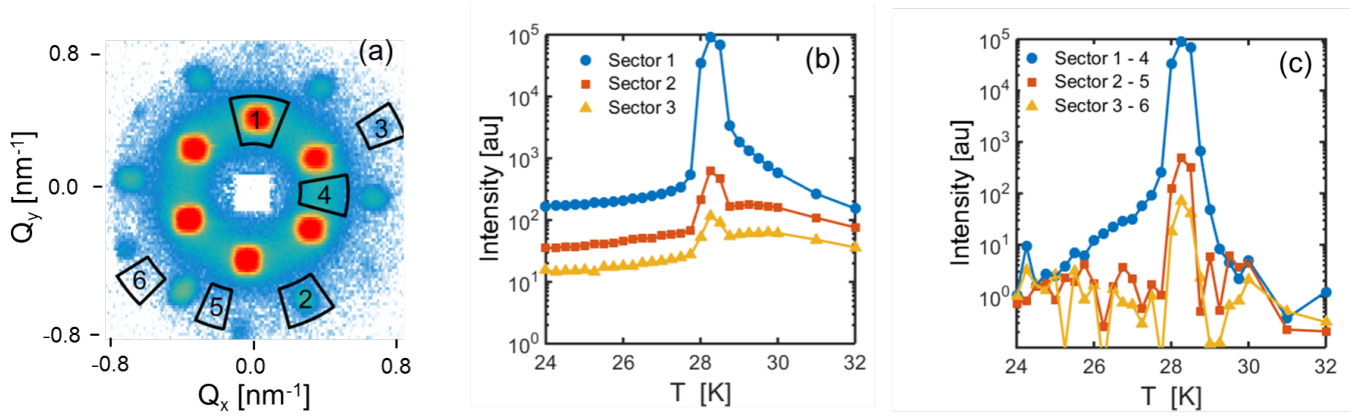


FIG. S1. Analysis of the peaks in the SANS patterns of the A-phase. (a) SANS pattern of MnSi in the A-phase for $B = 0.18$ T and $T = 28.5$ K where the different sectors used for the analysis are indicated. Sectors 1-3 correspond to the peaks of the Skyrmion lattice, with a 60 degrees periodicity due to the six-fold symmetry. The cut-off seen at $Q = 0.78 \text{ nm}^{-1}$ is due to the finite opening of the magnet. (b) Evolution of the intensities of Sectors 1-3 as a function of temperature for $B = 0.18$ T. (c) Evolution of the intensities Sectors 1-3 as a function of temperature for $B = 0.18$ T after correction of the diffuse scattering. For this purpose, the intensity of sectors outside of the peaks at the same Q -range and scaled to have the same size (Sectors 4-6) has been subtracted from the peak intensity.

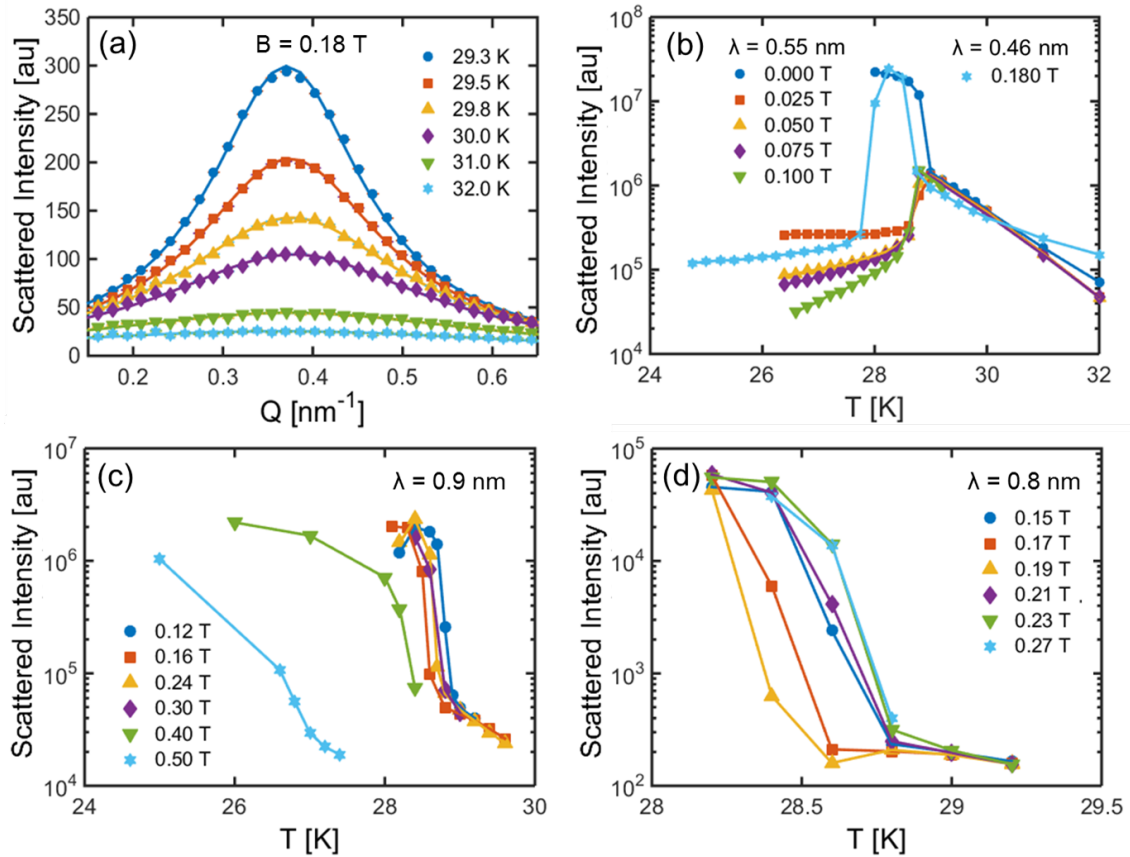


FIG. S2. (a) Plot of the D33 scattered intensity as a function of the momentum transfer Q at a magnetic field of 0.18 T. The radial-averaged curves are fitted with a Lorentzian as given by equation 2. (b) Total scattered intensity as a function of temperature measured on D33 with the magnetic field applied along the incident beam ($\vec{B} \parallel \vec{k}_i$). (c) and (d) total scattered intensity as a function of temperature for several magnetic fields applied perpendicular to the incident neutron beam ($\vec{B} \perp \vec{k}_i$) measured on IN15 with incident wavelength of $\lambda = 0.9 \text{ nm}$ and 0.8 nm respectively.

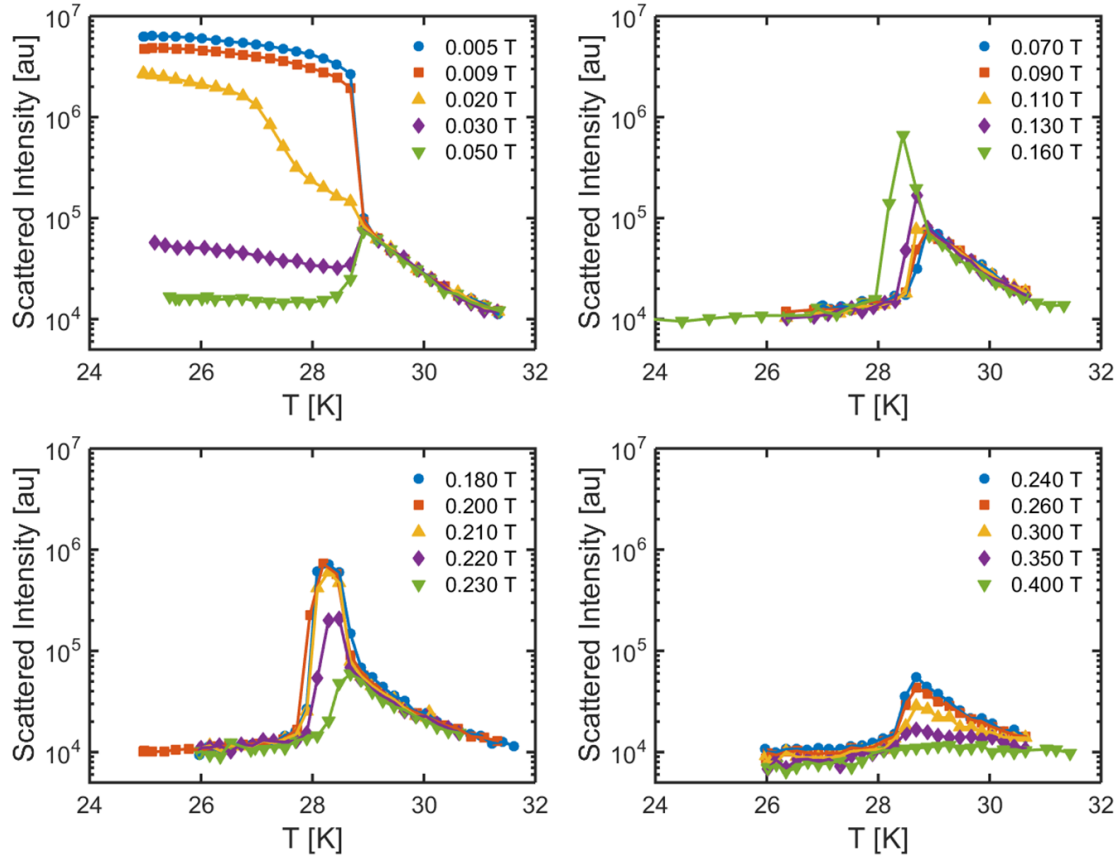


FIG. S3. Plot of the total scattered intensity as a function of temperature for twenty magnetic fields and $\vec{B} \parallel \vec{k}_i$ measured on IN15 with an incident wavelength of 0.8 nm.

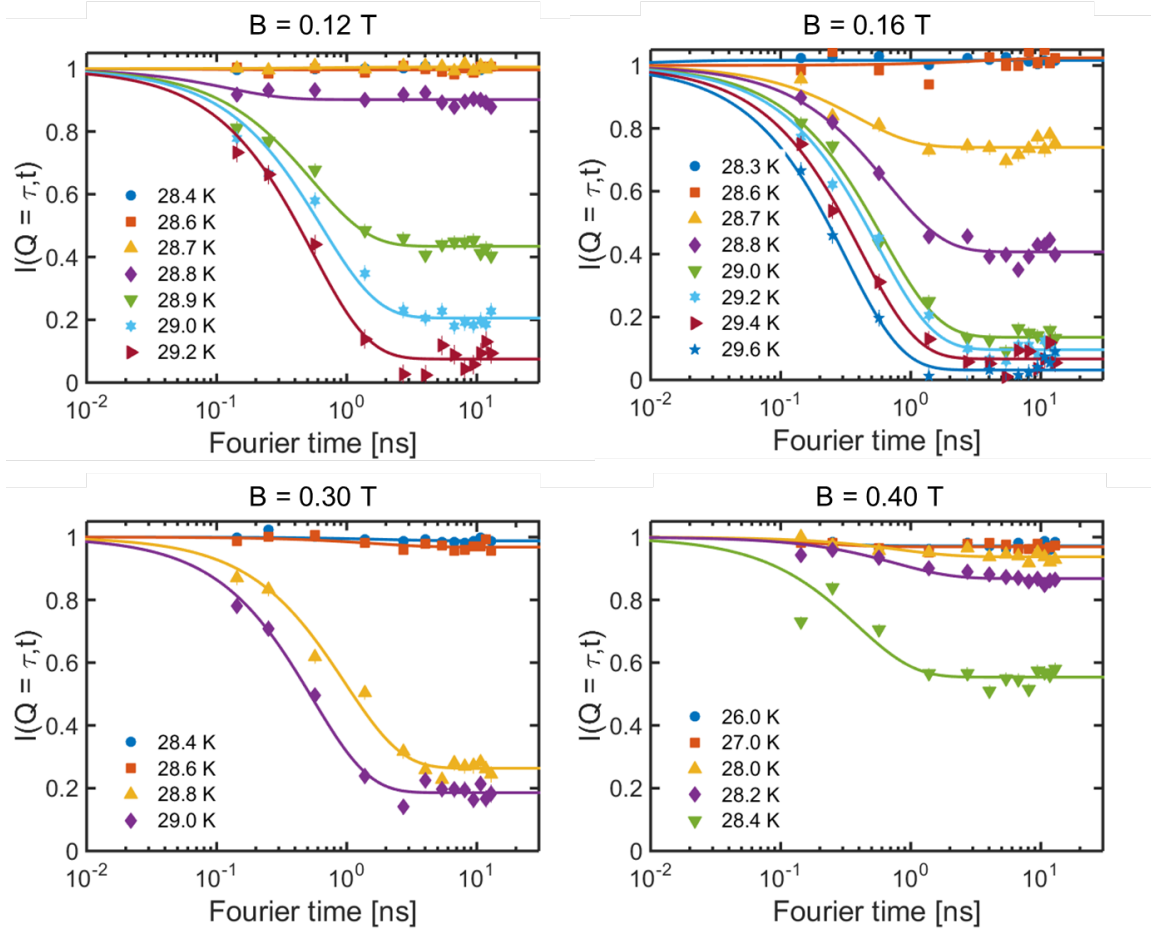


FIG. S4. Normalised intermediate scattering function $I(Q, t)$ measured with Neutron Spin Echo spectroscopy at four different magnetic fields measured on IN15 with an incident wavelength of 0.8 nm.